A Theoretical Thermodynamic Investigation of Cascade Reactions in Dinuclear Octa-azacryptates involving Carbon Dioxide

Morad M. El-Hendawy, Niall J. English* and Damian A. Mooney

The SFI Strategic Research Cluster in Solar Energy Conversion and the Centre for Synthesis and Chemical Biology, School of Chemical and Bioprocess Engineering, University College Dublin, Belfield, Dublin 4, Ireland.

This paper investigates the thermodynamics of gas-phase CO_2 cascade uptake-reactions in the form of carbonate or methoxycarbonate anions in the host cavity of various dinuclear octa-azacryptates of *m*-$CH_2C_6H_4CH_2$ and 2,5-furano-spaced hosts, L^1 and L^2 cryptands, using density functional theory (DFT). The cascade process involves two stages, namely the formation of dinuclear cryptate complexes and the subsequent formation of either μ-carbonato cryptate complexes or μ-monomethylcarbonato cryptates. The geometric and electronic structures are also investigated to determine the parameters which affect the stability of the complexes. Natural bond orbital (NBO) analysis has been used to investigate the interactions between the trapped anion and its host. The ion selectivity has been studied in terms of the formation of dinuclear crypate complexes, while the basicity and nucleophilicity of cryptands towards Lewis acids have also been studied, and good agreement was found vis-à-vis available experimental data.

* Corresponding author: niall.english@ucd.ie

1. Introduction

Atmospheric CO_2 uptake and conversion into energy-rich organic compounds is catalysed naturally by the enzyme Rubisco (Ribulose-1,5-biphosphate–carboxylase/oxygenase), which is distributed widely in green plants and algae [1]. As a result of potentially alarming reports which link global warming to the steadily increasing concentration of anthropogenic CO_2 in the atmosphere, there is currently much effort underway to 'mimic' CO_2 fixation artificially [2-16]. Despite CO_2 being considered one of the most inexpensive and plentiful sources of carbon, it is also one of the most inaccessible, due in large part to its chemical inertness. Thus, if rendered possible, the chemical activation of CO_2 could help serve to reduce its level in the atmosphere, while at the same time allowing CO_2 to be exploited as a carbon feedstock for the production of useful organic compounds [2].

Many studies refer to the importance of host cavities in transition metal complexes as catalysts in taking up and activating CO_2 from air [3-14]. One such strategy of cryptand complexation was developed by Lehn and co-workers over 30 years ago [17], the central idea of which lies in the replacement of the first solvation shell of a cation by a surrogate shell of a three-dimensional caged ligand-like "cryptand" to enhance both the thermodynamic and kinetic stability of the product (the so-called "cryptate effect") [17]. This effect underlies the varied applications of cryptands; they can be utilized for detoxification, environmental remediation, hydrometallurgy, etc. [18]. However, polyazacryptands constitute good candidates for incorporation into ion-selective membrane responsive to transition or heavy-metal cations, while polyether cryptands are responsive to alkali metal cations [18].

The *bis-tren* cryptands of interest in this work, L^1 and L^2, are shown in Fig. 1. These cryptands are octamine cages consisting of two tripodal tetramine sub-units, linked covalently by given spacers ($-CH_2-CH_2-$). These ligands are able to bind firstly with two metal ions, then an anion such as carbonate anion, according to a cascade mechanism [5, 9, 19]. In homodimetallic complexes, each metal centre (M^{2+}) occupies a *tren* cavity (*i.e.*, a coordination number of 4). Accordingly, it behaves as a receptor for anions [19], which serves to fill the otherwise empty cavities and adopt their donor atoms for coordination with both metal centres, forming trigonal bipyramidal or octahedral geometry [9]. Recently, dinuclear azacryptates of *m*-$CH_2C_6H_4CH_2$ [5,

9] and 2,5-furano-spaced hosts [5], namely L^1 and L^2 (cf. Fig. 1), have shown somewhat different tendencies to catalyse CO_2-uptake reactions within the sterically–protected host cavities which form homodinuclear μ-carbonato cryptates. Although the host molecules L^1 and L^2 exhibit a similar structure, carbonato-complexes of L^1 display further reactivity with primary alcohol-forming carbonate monoesters [5, 9], while those of L^2 do not. The failure of L^2 to do so may lie in the insufficient spacing between the pair of transition metals to accommodate the monomethyl ester [9].

The cascade reaction of CO_2 uptake takes place in two stages:

(i) Formation of a dinuclear cryptate by encapsulation of two transition metal cations in the host cavity of the cryptand (*L*). The metal cations of concern here are of the late first-row transition elements (from Co^{2+} to Zn^{2+}):

$$2M^{2+} + L \xrightarrow{\Delta G_1} [M_2L]^{4+} \quad (1)$$

(ii) Encapsulation of an anion in the host cavity of the dinuclear cryptate. Here, the carbonate anion may originate from a pre-formed carbonate or from the atmosphere. In the latter case, CO_2 reacts with the aqueous solution surrounding the dinuclear cryptate and forms CO_3^{2-}. Then the dinuclear cryptate uptakes the CO_3^{2-} anion, forming homodinuclear μ-carbonato cryptates:

$$[M_2L]^{4+} + CO_3^{2-} \xrightarrow{\Delta G_2} [M_2LCO_3]^{2+} \quad (2)$$

It is found that the replacement of the aqueous medium by methanol leads to the direct formation of monomethyl ester only in the case of the L^1 cryptand according to reaction (3) below [5, 9]:

$$[M_2L^1]^{4+} + CO_2 + MeOH \xrightarrow{\Delta G_3} [M_2L^1MeCO_3]^{3+} + H^+ \quad (3)$$

Or, it can be simplified to the overall reaction:

$$[M_2L^1]^{4+} + MeCO_3^- \xrightarrow{\Delta G_3} [M_2L^1MeCO_3]^{3+} \quad (4)$$

This means that replacement of one H atom of water by a methyl group (as in methanol) has a positive impact, because one C atom from CO_2 is added to another C atom from methanol. This behaviour has been reported for other complexes in the literature [14]. This indicates the possibility of the utility of cryptate complexes for the production of chemical feedstock.

The ultimate goal of this work is to provide a quantum-based understanding of the complexation reactions (discussed above) and to also investigate the effects, if any, that the metal ion may have. This is achieved by the calculation of Gibbs free energies and enthalpies of the gas-phase reactions described by schemes 1-3. An interesting question to consider is the relative selectivity of the cryptand towards the transition metal ion. These results have a direct impact on the cavity size and reactivity of the formed cryptate towards reaction with anionic substrates. This may be understood by considering the following:

$$2[M(H_2O)_6]^{2+} + [\acute{M}_2L]^{4+} \xrightarrow{\Delta\Delta G_{M\acute{M}}} [M_2L]^{4+} + 2[\acute{M}(H_2O)_6]^{2+} \quad (5)$$

It is expected that because both cryptands have very similar structure, their stability would be very close. Therefore we have studied their global and local nucleophilicity and basicity to show the affinity of both cryptands towards reaction with a Lewis acid.

2. Methodology

Single-crystal structures of cryptands and their complexes were obtained from the Cambridge Structural Database (CSD), where available. The referenced sources for the coordinates of cryptands L^1 and L^2 are refs. [20, 21]. The CCDC reference numbers of the carbonato cryptate complexes were 181027, 181029, 181031 and 181034 for Cu, Ni, Co and Zn in conjunction with L^1-based carbonato cryptate complexes, respectively, and 181032 for Co with the L^2-based complex. Because of the unavailability of X-ray structures of Ni, Cu and Zn cryptates of L^2, we have employed the results of other experimental analysis tools that suggest that they have similar structures to $[CoL^2CO_3]^{2+}$ [9]. Thus, these were derived here from their analogues by replacement of Co atoms with Ni, Cu or Zn atoms. Because of the unavailability of the coordinates of homo-dinuclear cryptates, they were derived from the corresponding carbonato-

bridged cryptates by dropping out the carbonate anion in the initial structures. However, the CCDC reference numbers of L^1-based methylcarbonato-bridged cryptates in the case of Cu, Ni and Zn were 181028, 181030 and 181033, respectively. The initial structure of the Co-derivative was taken from the analogous Ni form. In this work, all interfering species, such as residual solvents, were removed from the crystal structure before the calculations. Counter-ions were not considered due to computational intractability.

All calculations were performed using the Gaussian 09 suite [22], using density functional theory (DFT) in conjunction with the B3LYP functional [23-25]. Among quantum chemical methods for computational modelling of macrocyclic ligands and their complexes, DFT has been successfully applied to the calculation of the thermodynamic parameters for the cryptate formation reaction [26-28]. Since hydrogen atoms usually have low X-ray scattering factors and, as a result, their coordinates are not generally determined, structures from crystal data were subject to proton optimisation at the B3LYP/6-31G(d) level, with the coordinates of heavy atoms fixed. Because the interested complexes include open shell transition metal cations (Co^{2+}, Ni^{2+} and Cu^{2+}), they possess number of different spin states. Therefore, it is necessary to know the energy of these states. The closed-shell singlet and open-shell triplet (quintet and septet if any) states, as well as the antiferromagentic singlet states, have been optimized at either the RB3LYP/6-311+G(d,p) or UB3LYP/6-311+G(d,p) level. Although the energetic differences among these states are not great, we found the antiferromagentic state is the lowest in energy (cf. Table S1). This result agrees with the magnetic measurement of these complexes [9]. Therefore, we used this state to represent the studied complexes in this paper. However, the dinuclear zinc complexes have closed 3d-shell, thus closed-shell singlet states are used to model these at the RB3LYP/6-311+G(d,p) level. Frequency calculations were carried out to verify that structures were indeed optimised to their energy minima (*i.e.*, without any imaginary frequency components). In addition, natural bond orbital (NBO) analysis was undertaken using the NBO 3.1 program [29], as implemented in Gaussian 09.

Because cryptands act as nucleophilic ligands in the reaction of a Lewis acid (*i.e.*, either hydrogen protons or transition metal cations), global and local nucleophilicities were estimated according to the following procedure. The global nucleophilicity (N) is the reciprocal electrophilicity (ω), which is calculated using the following equation [30]:

$$N = \frac{1}{\omega} \quad \text{where} \quad \omega = \frac{\mu^2}{2\eta} \tag{6}$$

where μ is the electronic chemical potential and η is the chemical hardness. These two parameters were calculated using the vertical ionisation potential and electron affinity; for further details, see ref. [31]. To evaluate the nucleophilic power of the reactive sites within the molecule, a local nucleophilicity index was evaluated using the following equation [30]:

$$N^{-}(r) = N * f_k^{-} \tag{7}$$

where f_k^- is the Fukui function for electrophilic attack (*e.g.*, Lewis acid) on the nucleophilic sites (*e.g.*, the nitrogen atoms in the cryptand):

$$f_k^- = q_k(N) - q_k(N-1) \tag{8}$$

where $q_k\,(N)$ and $q_k(N-1)$ are the atomic population of atoms within the molecular species of *N* and *N*-1 electrons, respectively. This is discussed in further detail in ref. [31].

3. Results and discussion

3.1. Cryptands

Here, we consider the cryptands L^1 and L^2 prior to reaction with the metal ions. The optimized structures of L^1 and L^2 are shown in Fig. 1, together with their molecular structure. Geometry-optimised structural parameters are in good agreement with structural parameters determined by X-ray crystallography (cf. Supplementary Information, Table S2). The RMSD between the theoretical and experimental structures for L^1 and L^2 are small at 0.837 and 0.166 Å, respectively, with most structural deviation arising from the position of the hydrogen atoms.

Table 1 considers the natural population analysis (NPA) and local nucleophilicity of the nitrogen atoms in the cryptands. It is apparent that the charges on the bridgehead nitrogen atoms N1 and N5 are less than those of the other nitrogen atoms. For example, the NPA charge on the tertiary bridgehead nitrogen atoms of L^1 is less than the other nitrogen atoms by 12%. This agrees qualitatively with the previous experimental study that investigated the basicity of L^1 and

L^2 [21]. It is found that although the ligands have eight potential protonation sites, only six stepwise protonation constants could be determined which refer to six secondary amines, while the bridgehead amines remained undetectable [21]. The symmetric charge distribution on nitrogen atoms in each *tren* of L^1 is readily apparent, indicating parallel symmetry in the structure and reactivity. Replacement of phenyl rings by furanyl ones disrupts this symmetry. Results in Table 1 also suggest that NPA charges and local nucleophilicities on oxygen atoms of L^2 are much less than nitrogen atoms. This reflects the weak propensity of the oxygen atoms in furan rings to react with metal cations, in comparison to nitrogen atoms. This agrees with experimental observations which demonstrate that oxygen atoms do not share in the bonding with the metallic centres [21]. However, the local nucleophilicity of N1 and N5 in the cryptand, especially L^2, is higher than the other atoms, and hence the bonds between these atoms and metal ion would be formed more readily.

Besides the local parameters, the global nucleophilicity and proton affinity of the cryptands are also calculated (cf. Table 2). The proton affinity of a molecule is a measure of its gas-phase basicity, *i.e.*, the energy released in the following reaction:

$$L + 6H^+ \rightarrow [LH_6]^{6+} \quad (9)$$

The proton affinity of the ligand (L) is the negative value of the enthalpy change in the above reaction. Although nucleophilicity and basicity are very similar properties, it is generally accepted that nucleophilicity is a kinetic concept (i.e., characteristic of a rate constant) while basicity is a thermodynamic one [32]. Although basicity is related to the position of an equilibrium reaction with a proton, a good nucleophile is one that forms a new bond rapidly between a base and a proton (H^+) [32]. Table 2 shows the calculated global nucleophilicity and proton affinity together with the overall experimental basicity of L^1 and L^2. It is clear that L^1 is a better nucleophile and also a better base than L^2. This may be attributed to the lower basicity of the furanyl rings incorporating L^2 compared to the phenyl ones in L^1. The ratio between the calculated proton affinities of L^1 and L^2 is 1.02, which is the same the ratio between the overall experimental basicities of L^1 and L^2, aiding confidence as to the reliability of our results.

3.2. Dinuclear cryptates $[M_2L]^{4+}$

Despite there being no published crystallographic structures for the dinuclear cryptates, experimental studies confirm their existence [21, 33, 32]. Therefore, quantum techniques should be able to provide useful insights into the structure of these compounds. The lengths of metal-nitrogen bonds are around 2 Å (cf. Table S3). Meanwhile, Fig. 2 shows the optimized structure of $[Cu_2L^1]^{4+}$ as a representative example. As shown, each cation bonds in an enhedral manner into each *tren* cavity, forming a distorted tetrahedron in which the bridgehead tertiary nitrogen is perpendicular to a triangle of three secondary amino donors. All dinuclear cryptates of interest exhibit the same coordination pattern. However, the distance between the encapsulated metal-pair represents the cavity size in which the carbonate or the monomethylcarbonate anion would be trapped. This depends on the nature of the encapsulated metal cation; for instance, the cavity size in L^2-based dinuclear cryptates increases as the ionic radius of metal increases while the size in L^1-based dinuclear cryptates exhibits the reverse trend, as shown in Fig. 3. This shows the effect on the chemical structure of replacement of an m-benzene ring by furanyl one. However, this replacement led to a more compact structure of the host; for instance, the metal-metal distance drops from about 6.6 Å in the case of $[M_2L^1]^{4+}$ complexes to about 6.1 Å for $[M_2L^2]^{4+}$ complexes.

Nelson and co-workers have attempted to study the binding properties of dinuclear cryptates of L^1 and L^2 with late first-row transition metals from Co^{2+} to Zn^{2+}, but unfortunately L^1-dinuclear complexation was not observed, except in the case of Cu^{2+} [21]. This contrasts with other studies which confirm the formation of $[Co_2L^1]^{4+}$ [33] and $[Ni_2L^1]^{4+}$ [34]. It was also found that L^2 generally forms dinuclear cryptates with all transition metals of interest except in the case of Co^{2+} [21]. As a result, there is no complete picture of the binding properties of these cryptands with transition metal cations. In order to elucidate this matter, we have calculated the Gibbs free energy and enthalpy changes for the complexation reactions in the gas phase at standard conditions according to scheme (1).

There are three approaches for the calculation of thermodynamic parameters of metal-ligand complexation reactions in the gas phase. The first one is to consider the bare metal according to scheme (1) and this is the most popular [26]. The second considers a solvated metal cluster, such as hexa-aqua metal complex $[M(H2O)_6]^{2+}$, instead of the bare metal [27]. The third approach combines the first two [28], wherein the first step is the desolvation of the metal ion according to

scheme (11) and the second is the bare metal reaction with the cryptand as in scheme (1). Then, the free energy of the reaction is the sum of both steps ($\Delta G_1 + \Delta G_{desolv}$).

$$[M(H_2O)_6]^{2+} \xrightarrow{\Delta G_{desolv}} 2M^{2+} + 6H_2O \quad (10)$$

We have calculated the thermodynamic parameters using the three approaches. We found that the first approach works best because it correlates with available experimental data. Therefore, we discuss here only the results of the first approach; the reader is referred to the supplementary information for the other approaches. Table 3 lists the free energy and enthalpy of complexation reactions described in scheme (1) with and without the basis set superposition errors (BSSE). The BSSE is calculated using the counterpoise method [35]. It is apparent that BSSE does not affect the relative stability of complexes. The stability sequence of dinuclear cryptates has the same order, *i.e.*, $Cu2^+ > Zn^{2+} > Ni^{2+} > Co^{2+}$, for both ligands. This order agrees with the available experimental results as shown in Table 3. However, as seen, the stability of dinuclear cryptate do not depend greatly on the nature of cryptand with the same metal. For example, the free energy changes ΔG_1^{BSSE} for $[Cu_2L^1]^{4+}$ and $[Cu_2L^2]^{4+}$ are -562 and -563, respectively. Therefore, we could conclude that the effect of metal on the stability of dinuclear cryptate is very prominent compared to the nature of cryptand.

Because of the previously mentioned applications of cryptands, especially in the extraction of metal ions from an aqueous phase to an apolar organic phase [36], it is important to evaluate the relative binding selectivity to examine the feasibility of extraction. This is the difference in the free energy change $\Delta\Delta G_{M\acute{M}}$, as given by eqn. 5, using the following equations [28]. The experimental relative binding selectivity can be expressed as:

$$\Delta\Delta G^{exp}_{M,\acute{M}} = -2.303RTlog\frac{\beta}{\acute{\beta}} \quad (11)$$

where β and $\acute{\beta}$ are the overall binding constants. The theoretical relative binding selectivity is calculated as the difference in free energy changes specified in eqn. 5:

$$\Delta\Delta G^{theory}_{M,\acute{M}} = \Delta G_M - \Delta G_{\acute{M}} \quad (12)$$

Table 4 displays the relative binding selectivity between each couple of different metal ions where the first metal ion is solvated with the first solvated shell of water simulated in the aqueous medium and the second metal cation is encapsulated in the cryptand resembling an organic medium. The negative value of the relative binding selectivity is an indication of the feasibility of extraction of the first metal from the aqueous medium. Therefore, the selectivity of L^1 or L^2 towards the Cu^{2+} cation is superior in terms of selectivity vis-à-vis other transition metal cations of interest. This is in agreement with previously reported experiments [21].

3.3. Dinuclear carbonato-bridged cryptates $[M_2LCO_3]^{2+}$

It is well-known that the carbonate bridge in dinuclear metal complexes has five different coordination modes depending on the nature of metal and the cavity size [37], as illustrated in Table 5. Because of the high degree of flexibility in the geometry of cryptates, it is important that the techniques used here are able to demonstrate agreement. Actually, DFT-generated geometries of dinuclear carbonato-bridged cryptates exhibit the same coordination modes (***a***, ***b***, and ***e***) as those obtained from experiment (cf. Table 5). The optimised geometries of $[Zn_2L^1CO_3]^{2+}$, $[Cu_2L^1CO_3]^{2+}$ and $[Ni_2L^2CO_3]^{2+}$ are shown in Fig. 4 as representative examples for coordination modes of ***a***, ***b***, and ***e,*** respectively. Complexes with mode ***b*** have trigonal-bipyramidal structure for each metallic centre where the bridgehead nitrogen and one oxygen donor are orthogonal on the face of triangle for which the positions of N2, N3 and N4 constitute its corners. The situation is different in the case of $[Zn_2L^1CO_3]^{2+}$ (mode ***a***). While the Zn9 atom embeds in a trigonal-bipyramid arrangement, Zn10 is embedded in a square-pyramid structure. Complexes with mode ***e*** have distorted octahedral geometries around each metallic centre. For example, the Ni9 centre in $[Ni_2L^2CO_3]^{2+}$ is embedded in an octahedral motif in which N2 and N4 positions are semi-orthogonal on a square planar geometry consisting of O12, O14, N1 and N3 atoms. In such cases, the carbonate anion acts as a bidentate ligand, the centre of which may confer extra stability to the complex compared to those of the other modes. However, the other calculated structural parameters, such as bond length and angle, are in satisfactory agreement with the corresponding published X-ray parameters (cf. Tables S5 and S6). The average percentage errors in bond lengths between these calculations and available x-ray data were 0.86%, 0.65%, 1.12%

and 0.96% for Co^{2+}, Ni^{2+}, Cu^{2+} and Zn^{2+} L^1-based μ-carbonato cryptates, respectively. For the case of dicobalt μ-carbonato cryptate (the only one for which experimental structural data is available), the average errors in bond lengths were 1.60%. In terms of critical angles, calculated percentage errors were 3.46%, 5.14%, 1.50% and 6.75% for Co^{2+}, Ni^{2+}, Cu^{2+} and Zn^{2+} L^1-based μ-carbonato cryptates, respectively. Again, for the case of dicobalt μ-carbonato cryptates (the only one for which experimental structural data is available), the average errors in angles were 0.92%. At this point, structural replication was deemed to be of sufficient quality to proceed. An example of the utility of the techniques used here is the good correlation between the experimental and calculated metal-metal distance of $[M_2L^1CO_3]^{2+}$ (cf. Fig. 5). Another interesting observation is the shortening M...M distance in $[M_2L^2CO_3]^{2+}$ compared to $[M_2L^1CO_3]^{2+}$ which yields more compact structures. For example, while the M...M distance in $[M_2L^1]^{4+}$ and $[M_2L^2]^{4+}$ complexes hovers around 6.6 and 6.1 Å, the encapsulation of CO_3^{-2} anion in these complexes serves to reduce these to about 5.5 and 4.4 Å, respectively. This is attributed to the arrangement of the carbonate anion (mode ***e***) which interacts with each metallic centre as a bidentate ligand. In such cases, the negative carbonate anion attracts two positive centres leading to a more compact structure. However, the stronger drop in M...M distance in the case of the $[M_2L^2CO_3]^{2+}$ complexes is ascribed to the use of CO_3^{-2} anion to affect the bidentate character in the interaction with the two positive centers. These observations agree with previous experimental results [9].

It is noteworthy that, compared to L^1-based complexes, the binding of CO_3^{2-} anion with L^2-based complexes are thermodynamically favourable, where the bidentate bonding of carbonate anions with each metallic centre in the latter case confers extra stability. However, the stability sequence of dinuclear carbonato-bridged cryptates depends on the binding mode of carbonate anion (cf. Table 6). For instance, the stability sequence of $[M_2L^1CO_3]^{2+}$ complexes is $Co^{2+} > Zn^{2+} > Cu^{2+} > Ni^{2+}$, while for $[M_2L^2CO_3]^{2+}$ complexes, it is $Ni^{2+} > Co^{2+} > Zn^{2+} > Cu^{2+}$. However, the BSSE is important in defining the relative stability among for $[M_2L^1CO_3]^{2+}$ complexes. For example, the ΔG_2 values for Cu and Zn-complexes are equal at -624 kcal/mol, but by considering the BSSE, their ΔG_2^{BSSE} values became -595 and -601 kcal/mol, respectively. There is no clear-cut relationship between the stability of the complex and the cavity size or ionic radius, but they have effects to some extent. For example, on going from Ni to Zn-complexes of $[M_2L^1CO_3]^{2+}$,

the ΔG_2^{BSSE} value increases by decreasing the M...M distance and increasing the ionic radius of the metal.

The orbital bonding interactions between metal ions and carbonate anion can be examined by the NBO method [38]. The second-order perturbation energy, E(2), arises between the filled molecular orbital as a donor (i) and the neighbouring empty molecular orbitals as acceptor (j). E(2), termed the stabilisation energy associated with the delocalisation occurring between the donor NBO (i) and the acceptor NBO (j) - 2e stabilisation, can be estimated from the following equation:

$$E(2) = \Delta E_{ij} = q_{i.} F^2(i, j)/(\varepsilon_j - \varepsilon_i) \quad (13)$$

where q_i is the i-th donor orbital occupancy, ε_i and ε_j are the diagonal elements (orbital energies) and $F(i,j)$ is the off-diagonal NBO Fock matrix element [38]. As a rule, the greater the value of E(2), the stronger the interaction between a donor NBO and an acceptor NBO. Therefore, E(2) is used to assign and evaluate orbital contributions for stabilising the complex structures under investigation. Tables 7 and 8 show the E(2) of μ-carbonato cryptate complexes. In NBO analysis, the natural bond orbitals are defined for each covalent bond, lone pair and anti-bonding orbital. Among the possible interactions between each two NBOs, the interaction between the lone pair of the O atom of the carbonate anion and the *3d*-antibonding orbital contribute significantly to the stabilization of the complex. The summation of E(2), namely $\sum E^{(2)} donor \rightarrow acceptor$ [39], gives a good correlation with the stability of complex. It is apparent that $\sum E^{(2)}$donor → acceptor is larger for $[M_2L^2CO_3]^{2+}$ complexes than $[M_2L^1CO_3]^{2+}$ ones, which confirms the bidentate action of carbonate anions for adding extra stability to the former.

3.4. Dinuclear μ-monomethylcarbonato cryptates $[M_2L^1MeCO_3]^{3+}$

It is well known that the reaction of CO_2 with hydroxide to generate bicarbonate or carbonate ions is extremely slow in the absence of a catalyst. However, it was reported that dinuclear transition metal complexes are able to uptake atmospheric CO_2 and then catalyse it to form carbonate or bicarbonate [13, 40, 41]. The dimetallic cryptates of L^1 under ambient atmospheric

conditions forms methylcarbonato-bridged cryptates in methanolic solution [9]. The forming of such compounds is considered evidence of the ability of dinuclear cryptates to activate CO_2 and increasing the number of carbon atoms by reaction with methanol. This would be considered highly beneficial for producing chemical feedstock compounds.

In this work, the geometries of all methylcarbonato-bridged cryptates of L^1 were optimized using B3LYP/6-311+G(d,p) method based on the available X-ray coordinates [9]. The calculation showed that the antiferromagentic species have the lowest energies which agree with the experimental finding [9]. The monomethylcarbonate fragment has syn-anti μ-η_1, η_2 arrangement within the host cavity of the dinuclear cryptates (see Fig. 6 as a representative example). Table S7 lists some selected bond length and bond angles together with the corresponding X-ray data, if available; it is apparent that there is general agreement with those of the crystal structures. The average percentage errors in bond lengths between these calculations and available x-ray data were 1.20%, 2.26% and 0.79% for Ni^{2+}, Cu^{2+} and Zn^{2+}, respectively, while the average respective percentage errors in the critical angles, for which the expected flexibility is higher, were 0.15%, 1.1% and 0.25%. An interesting example for this agreement was that both the available experimental and theoretical metal-metal distances in the series have the same trend: $Zn^{2+} > Cu^{2+} > Ni^{2+} > Co^{2+}$. This order depends on the population of 3d-orbitals of the metal cation. On the other hand, the calculated free energies and enthalpies of binding for $[M_2L^1MeCO_3]^{3+}$ reveal that the strength of binding of dimetallic cryptate with monomethylcarbonate fragment follows the trend: $Cu^{2+} > Zn^{2+} \approx Ni^{2+} > Co^{2+}$, as shown in Table 9; this trend is similar to that of the dinuclear cryptates, but with lower stability. In other words, the encapsulation of the monomethylcarbonate anion destabilizes the monomethylcarbonato cryptates by about 208 kcal/mol while the encapsulation of carbonate anion stabilizes it by about 90 kal/mol. On the other hand, the negative enthalpy and free energy of the reactions for dinuclear cryptate with the carbonate or monomethylcarbonate anion reflects their exothermic and spontaneous formation, in accord with experimental observations [9].

In order to describe the orbital interaction between the monomethylcarbonate fragment and metallic cations in the dinuclear cryptate, NBO analysis was conducted and the results are presented in Table 10. Here, one can see that the interaction between the lone pairs of oxygen atoms in monomethylcarbonate and the antibonding *3d*-orbitals of metal cations contribute

significantly to the stabilisation of complexes. However, the overall orbital interaction between monomethylcarbonate fragment and the dinuclear cryptate $\sum E^{(2)} donor \rightarrow acceptor$ follows the same trend of the overall stability of the complexes. This indicates the significant dependence of stability of complexes on these orbital interactions.

4. Conclusions

In conclusion, the DFT geometries of studied cryptands and their complexes are in reasonable agreement with the available X-ray crystallographic data. Also, the calculations have reproduced the arrangement mode of carbonate and methoxycarbonate anion in the host cavity of dinuclear cryptate. The global nucleophilicity and proton affinity of L^1 cryptand is larger than L^2 towards the Lewis acid which agrees with experimental findings. In addition, L^1 and L^2-based dinuclear cryptates have comparable stability with the same metallic centres. However, the sequence of stability is the same for both types, Cu^{2+}> Zn^{2+}> Ni^{2+}> Co^{2+}, in accord with experimental data. It was also found that the mode of arrangement of the carbonate anion in the host cavity of the dinuclear cryptate affects the stability of the complex significantly. The results demonstrate that the reaction of the dinuclear cryptate with carbonate anion is more thermodynamically favourable than that with methoxycarbonate anion. Finally, the stability of the carbonato or monomethylcarbonato cryptates depends generally on the cavity size where the anionic fragment would be trapped and the ionic radius of the metal cation as well.

Acknowledgements

The authors acknowledge useful conversations with Dr. Grace Morgan. This material is based upon works supported by Science Foundation Ireland (SFI) under Grant No. [07/SRC/B1160]. We also thank SFI and the Irish Centre for High-End Computing for the provision of high-performance computing facilities.

References

1. Andrews TJ, Lorimer GH (1987) Rubisco: structure, mechanisms and prospects for improvement. In The Biochemistry of Plants; Eds. Hatch MD, Boardman NK Academic Press: New York 10:131-218.
2. Aresta M, Dibenedetto A (2007) Utilization of CO_2 as a chemical feedstock: opportunities and challenges. Dalton Trans 2975-2992 and references therein.
3. Kong LY, Zhang ZH, Zhu HF, Kawaguchi H, Okamura T, Doi M, Chu Q, Sun WY, Ueyama N (2005) Copper(II) and zinc(II) complexes can fix atmospheric carbon dioxide. Angew Chem 117:4426–4429.
4. Kersting B (2001) Kohlendioxid-Fixierung an Zweikernkomplexen mit hydrophoben Bindungstaschen Angew Chem 113: 4109–4112.
5. Chen JM, Wei W, Feng XL, Lu TB (2007) CO_2 fixation and transformation by a dinuclear copper cryptate under acidic conditions. Chem Asian J 2:710-719.
6. Kong LY, Zhu HF, Huang YQ, Kawaguchi H, Lu XH, Song Y, Liu GX, Sun WY, Ueyama N (2006) cadmium(II) and copper(II) complexes with imidazole-containing tripodal polyamine ligands: pH and anion effects on carbon dioxide fixation and assembling. Inorg Chem 45:8098–8107.
7. Verdejo B, Aguilar J, Espana EG, Gavina P, Latorre J, Soriano C, Llinares JM, Domenech A (2006) CO_2 fixation by Cu^{2+} and Zn^{2+} complexes of a terpyridinophane aza receptor. Crystal structures of Cu^{2+} complexes, pH-metric, spectroscopic, and electrochemical studies. Inorg Chem 45:3803–3815.
8. Derossi S, Bond AD, McKenzie CJ, Nelson J (2005) (μ_2-Bicarbonato-κ^2O,O')[μ_2-1,4,8,11,14,18,23,27-octaaza-6,16,25(1,3)-tribenzenabicyclo[9.9.9]nonacosaphane] dicopper(II) triperchlorate acetonitrile solvate. Acta Crystallogr Sect E, 61:m1379–m1382.
9. Dussart Y, Harding C, Dalgaard P, McKenzie C, Kadirvelraj R, McKee V, Nelson J (2002) Cascade chemistry in azacryptand cages: bridging carbonates and methylcarbonates J Chem Soc Dalton Trans. 1704–1713.
10. Bazzicalupi C, Bencini A, Bencini A, Bianchi A, Corana F, Fusi V, Giorgi C, Paoli P,Paoletti P, Valtancoli B, Zanchini C (1996) CO_2 fixation by novel copper(ii) and

zinc(II) macrocyclic complexes. a solution and solid state study. Inorg. Chem. 35:5540–5548.

11. Paddock RL, Nguyen ST (2001) Chemical CO_2 fixation: Cr(III) salen complexes as highly efficient catalysts for the coupling of CO_2 and epoxides. J Am Chem Soc 123:11498-11499.
12. Escuer A, Mautner F A, Penalba E, Vicente R (1998) Superexchange Pathway for the Different Coordination Modes of the Carbonato Bridge in Polynuclear Copper(II) Compounds. Inorg Chem 37:4190–4196.
13. Kitajima N, Hikichi S, Tanaka M, Moro-oka Y (1993) Fixation of atmospheric CO_2 by a series of hydroxo complexes of divalent metal ions and the implication for the catalytic role of metal ion in carbonic anhydrase. synthesis, characterization, and molecular structure of $[LM(OH)]_n$ (n = 1 or 2) and LM(.mu.-CO_3)ML (M(II) = Mn, Fe, Co, Ni, Cu, Zn; L = HB(3,5-iso-Pr2pz)3). J Am Chem Soc 115:5496–5508.
14. Kato M, Ito T (1986) Syntheses, characterization, and structures of (monomethyl carbonato)–nickel(ii), –copper(ii), and –cobalt(ii) complexes with tetraazacycloalkanes obtained from CO_2 uptake. Bull Chem Soc Jpn 59:285–294.
15. Kato M, Ito T (1985) Syntheses, characterization, and structures of (monomethyl carbonato)nickel(II), -copper(II), and -cobalt(II) complexes with tetraazacycloalkanes obtained from carbon dioxide uptake. Inorg Chem 24:504–508.
16. Kato M, Ito T (1985) Facile carbon dioxide uptake by zinc(II)-tetraazacycloalkane complexes. 2. X-ray structural studies of (.mu.-monomethyl carbonato)(1,4,8,11-tetraazacyclotetradecane)zinc(II)perchlorate,bis(.mu.-monomethylcarbonato)tris[(1,4,8,12-tetraazacyclopentadecane)zinc(II)] perchlorate, and (monomethylcarbonato)(1,4,8,11-tetramethyl-1,4,8,11-tetraazacyclotetradecane)zinc(II) perchlorate. Inorg Chem 24:509–514.
17. Lehn J-M (1978) Cryptates: inclusion complexes of macropolycyclic receptor molecules Pure Appl Chem 50:871-892 and reference therein.
18. Nelson J, McKee V, Morgan G. (1998) Coordination chemistry of azacryptands. In Progress in Inorganic Chemistry, Ed. Karlin KD Wiley, New York 47:191-192.

19. Amendola V, Fabbrizzi L, Mangano C, Pallavicini P, Poggi A, Taglietti A (2001) Anion recognition by dimetallic cryptates. Coord Chem Rev 219−221:821−837.
20. Arthurs M, McKee V, Nelson J, Town RM (2001) Chemistry in cages: dinucleating azacryptand hosts and their cation and anion cryptates. J Chem Ed 78:1269–1272.
21. Arnaud-Neu F, Fuangswasdi S, Maubert B, Nelson J, McKee V (2000) Binding properties of octaaminocryptands. Inorg Chem 39:573-579.
22. Frisch MJ, Trucks GW, Schlegel HB, et al. (2009), GAUSSIAN09, Revision A. 02, Gaussian, Inc., Wallingford, CT.
23. Becke AD (1993) Density-functional thermochemistry. III. The role of exact exchange. J Chem Phys 98:5648–5652.
24. Lee C, Yang W, Parr RG (1988) Development of the Colle-Salvetti correlation energy formula into a functional of the electron density Phys Rev B 37:785–789.
25. Stevens PJ, Devlin FJ, Chablowski CF, Frisch MJ (1994) Abinitio calculation of vibrational absorption and circular dichroism spectra using density functional force fields. J Phys Chem 98:11623–11627.
26. Wang X, Wang H, Tan Y (2008) DFT study of the cryptand and benzocryptand and their complexes with alkali metal cations: Li^+, Na^+, K^+ . J Comput Chem 29: 1423–1428.
27. Puchta R, Eldik RV (2007) Host–guest complexes of oligopyridine cryptands: prediction of ion selectivity by quantum chemical calculations. Eur J Inorg Chem 10:1120–1127.
28. Su JW, Burnette RR (2008) First Principles Investigation of Noncovalent Complexation: A [2.2.2]-Cryptand Ion-Binding Selectivity Study ChemPhysChem 9:1989-1996.
29. Glendening ED, Reed AE, Carpenter JE, Weinhold F NBO 3.1(2003) Program as implemented in the Gaussian 09 package.
30. Pratihar S, Roy S J. (2010) Nucleophilicity and Site Selectivity of Commonly Used Arenes and Heteroarenes. J Org Chem 75:4957-4963.
31. Chattaraj PK, Sarkar U, Roy DR (2006) Electrophilicity Index. Chem Rev 106:2065-2091.
32. Carey FA, Sundberg RJ (1990) Advanced Organic Chemistry, 3rd ed., Part A. Structure and Mechanisms. Plenum press: New York.

33. Menif R, Reibenspies J, Martell AE (1991) Synthesis, protonation constants, and copper(II) and cobalt(II) binding constants of a new octaaza macrobicyclic cryptand: (MX)3(TREN)2. Hydroxide and carbonate binding of the dicopper(II) cryptate and crystal structures of the cryptand and of the carbonato-bridged dinuclear copper(II) cryptate. Inorg Chem 30:3446: 3454.
34. Fabbrizzi L, Pallavicini P, Parodi J, Perotti A, Sardone N, Taglietti A (1996) A structurally characterized azidebridged dinuclear nickel(II*)* cryptate. Inorg Chim Acta 244:7-9.
35. Boys SF, Bernardi F (1970) The calculation of small molecular interactions by the differences of separate total energies. Some procedures with reduced errors. Mol Phys 19:553-566.
36. Khopkar SM, Basic Concepts of Analytical Chemistry", 2nd Edition (1998), New Age International Publications, New Delhi, pp 112-113.
37. Escuer A, Vicente R, Kumar SB, Solans X, Font-Bardía M (1997) A novel tridentate coordination mode for the carbonatonickel system. J Chem Soc Dalton Trans 403-408.
38. Reed AE, Curtiss LA, Weinhold F. (1988) Intermolecular interactions from a natural bond orbital, donor-acceptor viewpoint. Chem Rev 88:899-926.
39. Kovács A, Nemcsok DS, Kocsis T (2010) Bonding interactions in EDTA complexes. J. Mol. Str.: THEOCHEM 950:93-97.
40. Palmer DA, Van Eldik R (1983) The chemistry of metal carbonato and carbon dioxide complexes. Chem. Rev 83:651-731.
41. Rawle SC, Harding CJ, Moore P, Alcock NW (1992) Crystal structure of an antiferromagnetically coupled p-carbonato-bridged dinickel(II) complex containing the pendent-arm macrocycle I -(3-dimethylaminopropyl)-l,5,9-triazacyclododecane (L^1); a system which readily sequesters carbon dioxide from air. J Chem Soc Chem Commun 1701-1703.

Table 1. NPA charge (q) and local nucleophilicity (N_k^-) for key atoms in L^1 and L^2

Key site	$(q)_{L^1}$	$(q)_{L^2}$	$(N_k^-)_{L^1}$	$(N_k^-)_{L^2}$
N1	-0.60	-0.59	0.378	0.467
N2	-0.68	-0.68	0.373	0.307
N3	-0.68	-0.71	0.373	0.400
N4	-0.68	-0.68	0.372	0.308
N5	-0.60	-0.59	0.377	0.437
N6	-0.68	-0.69	0.374	0.315
N7	-0.68	-0.71	0.371	0.380
N8	-0.68	-0.68	0.374	0.307
O 11	---	-0.48	---	0.216
O12	---	-0.48	---	0.217
O13	---	-0.48	---	0.215

Table 2. The global nucleophilicity and proton affinity calculated in this work together with the experimentally measured overall basicity

	L^1	L^2
Global nucleophilicity	0.921	0.907
Proton affinity (-ΔH) Kcal/mol	680	611
Overall basicity ($\sum logK_i$)[a]	48.3 ± 0.8	44.2 ± 0.8

[a] the data is taken from ref. [21]; $\sum logK_i$ is the summation of the measured stepwise protonation constants.

Table 3. Binding Gibbs free energies and enthalpies with (ΔG_1^{BSSE}, ΔH_1^{BSSE}) and without (ΔG_1, ΔH_1) BSSE in kcal/mol in the gas phase at 298.15 K for (i) $[M_2L^1]^{4+}$ and (ii) $[M_2L^2]^{4+}$ complexes

(i)	**ΔG_1**	**ΔH_1**	**BSSE**	**ΔG_1^{BSSE}**	**ΔH_1^{BSSE}**	**Overall stability constant**
Co^{2+}	-467	-492	6.03	-460	-486	13.56[a]
Ni^{2+}	-513	-531	9.48	-495	-523	---
Cu^{2+}	-567	-593	5.67	-562	-588	26.20[a]
Zn^{2+}	-517	-544	6.68	-510	-537	---
(ii)	ΔG_1	ΔH_1	BSSE	ΔG_1^{BSSE}	ΔH_1^{BSSE}	---
Co^{2+}	-458	-489	3.77	-454	-482	9.75 ± 0.06[b]
Ni^{2+}	--496	-524	7.31	-489	-517	---
Cu^{2+}	-564	-592	1.48	-563	-590	25.38 ± 0.08[b]
Zn^{2+}	-514	-542	6.9	-507	-535	16.10 ± 0.01[b]

[a] and [b] refer to the data taken from refs. [21] and [33], respectively.

Table 4. Relative binding selectivity (kcal/mol) for L^1-based and L^2-based dinuclear cryptates according to the reaction described in eqn. 5

M^{2+}: $\acute{M}^{2+}$	$(\Delta\Delta G_{M\acute{M}})_{L^1}$	$(\Delta\Delta G_{M\acute{M}})_{L^2}$
Cu^{2+} : Co^{2+}	-87	--70
Cu^{2+} : Ni^{2+}	-11	-51
Cu^{2+} : Zn^{2+}	-2	-3
Ni^{2+} : Co^{2+}	--77	--19
Ni^{2+} : Zn^{2+}	201	240
Ni^{2+} : Zn^{2+}	277	260

Table 5. Different coordination modes of carbonate bridge in dinuclear metal complexes.

Mode symbol	***a***	***b***	***c***	***d***	***e***
Mode structure	*Syn- anti* η_1,η_1	*Anti-anti* η_1,η_1		μ-η_2,η_2	μ-η_2,η_2
Examples	$[Zn_2L^1CO_3]^{2+}$	$[Co_2L^1CO_3]^{2+}$ $[Cu_2L^1CO_3]^{2+}$ $[Ni_2L^1CO_3]^{2+}$	---	---	$[Co_2L^2CO_3]^{2+}$ $[Ni_2L^2CO_3]^{2+}$ $[Cu_2L^2CO_3]^{2+}$ $[Zn_2L^2CO_3]^{2+}$

Table 6. Binding Gibbs free energies and enthalpies with (ΔG_2^{BSSE}, ΔH_2^{BSSE}) and without (ΔG_2, ΔH_2) BSSE by kcal/mol in gas phase at 298.15 K together with M…M distance (experimental value in brackets) (Å) and ionic radius of metal cation (Å) for (i) $[M_2L^1CO_3]^{2+}$ (ii) $[M_2L^2CO_3]^{2+}$ complexes

(i)	**ΔG_2**	**ΔH_2**	**BSSE**	**ΔG_2^{BSSE}**	**ΔH_2^{BSSE}**	**M...M distance**	**Ionic radius**
Co^{2+}	-632	-646	27.36	-605	-619	5.817 (5.939)	0.67
Ni^{2+}	-606	-619	25.66	-580	-593	5.920 (6.018)	0.63
Cu^{2+}	-624	-640	28.87	-595	-611	5.752 (5.791)	0.65
Zn^{2+}	-624	-636	22.76	-601	-613	5.163 (5.331)	0.68
(ii)	**ΔG_2**	**ΔH_2**	**BSSE**	**ΔG_2^{BSSE}**	**ΔH_2^{BSSE}**	**M...M distance**	**Ionic radius**
Co^{2+}	-665	-682	25.83	-639	-656	4.406 (4.292)	0.65
Ni^{2+}	-683	-699	25.66	-657	-674	4.427	0.69
Cu^{2+}	-636	-649	27.80	-608	-621	4.336	0.73
Zn^{2+}	-639	-650	23.55	-616	-627	4.429	0.74

Table 7. Second-order perturbation interaction energies (E(2)) of $[M_2L^1CO_3]^{2+}$ complexes (kcal/mol) together with the orbital population of the metal cation given by electrons

Donor→Acceptor	**Co^{2+}**	**Ni^{2+}**	**Cu^{2+}**	**Zn^{2+}**
LP(O12)→LP*(M9)	63.83	63.50	37.80	47.75
LP(O13)→LP*(M10)	34.20	32.00	45.50	33.53
LP(O14)→LP*(M9)	5.00	6.00	4.00	6.01
LP(O14)→LP*(M10)	4.00	6.00	4.00	2.67
BD(C11-O12)→LP*(M9)	8.00	8.00	6.20	6.6
BD(C11-O13)→LP*(M10)	6.00	7.00	6.00	5.00
BD(C11-O14)→LP*(M9)	5.00	7.50	3.01	4.53
BD(C11-O14)→LP*(M10)	5.00	7.00	---	2.35
$\sum E^{(2)} donor \rightarrow acceptor$	131.03	137.00	106.51	108.44
Average population of M^{2+}	4s (0.23) *3d* (7.71)	4s (0.27) *3d* (8.66)	4s (0.25) *3d* (9.51)	4s (0.35) *3d* (9.99)

Table 8. Second-order perturbation interaction energies (E(2)) of $[M_2L^2CO_3]^{2+}$ complexes (kcal/mol) together with the orbital population of the metal cation given by electrons

Donor→Acceptor	**Co^{2+}**	**Ni^{2+}**	**Cu^{2+}**	**Zn^{2+}**
LP(O12)→LP*(M9)	46.76	46.36	14.83	45.14
LP(O13)→LP*(M10)	23.00	28.70	29.37	40.99
LP(O14)→LP*(M9)	26.35	20.33	19.60	2.86
LP(O14)→LP*(M10)	22.00	28.89	17.64	10.00
BD(C11-O12)→LP*(M9)	-7.00--	9.50	11.10	4.1
BD(C11-O13)→LP*(M10)	10.00	9.50	4.00	4.60
BD(C11-O14)→LP*(M9)	8.50	3.20	5.11	3.1
BD(C11-O14)→LP*(M10)	5.70	7.20	6.90	3.10
$\sum E^{(2)} donor \rightarrow acceptor$	142.31	153.68	108.55	113.09
Average population of M^{2+}	4s (0.23) *3d* (7.71)	4s (0.27) *3d* (8.66)	4s (0.25) *3d* (9.51)	4s (0.35) *3d* (9.99)

Table 9. Binding Gibbs free energies and enthalpies with (ΔG3BSSE, ΔH3BSSE) and without (ΔG3, ΔH3) BSSE in kcal/mol in gas phase at 298.15 K for [M2L1MeCO3]3+ complexes together with M…M distance (experimental value in brackets) (Å) and ionic radius of metal cation (Å)

	ΔG_3	**ΔH_3**	**BSSE**	**ΔG_3^{BSSE}**	**ΔH_3^{BSSE}**	**M...M distance**	**Ionic radius**
Co^{2+}	-271	-301	6.05	-264	-295	5.591	0.67
Ni^{2+}	-305	-334	6.47	-298	-327	5.648 (5.629)	0.63
Cu^{2+}	-342	-379	5.73	-336	-373	5.667 (5.655)	0.65
Zn^{2+}	-307	-335	6.62	-299	-328	5.888 (5.982)	0.68

Table 10. Second-order perturbation interaction energies (E(2)) of $[M_2L^1MeCO_3]^{3+}$ complexes (kcal/mol) together with the orbital population of the metal cation given by electrons

Donor→Acceptor	Co2+	Ni2+	Cu2+	Zn2+
LP(O12)→LP*(M9)	35.08	37.08	39.41	45.14
LP(O13)→LP*(M10)	16.01	19.01	26.84	40.99
LP(O14)→LP*(M9)	---	---	19.32	2.86
LP(O14)→LP*(M10)	13.9	8.46	---	---
BD(C11-O12)→LP*(M9)	---	---	8.7	4.1
BD(C11-O13)→LP*(M10)	14.53	11.53	6.3	3.1
BD(C11-O14)→LP*(M10)	11.13	17.5	9.29	---
$\sum E^{(2)} donor \rightarrow acceptor$	90.65	93.58	109.86	96.19
Average population of M2+	4S (0.23) 3d (7.73)	4S (0.23) 3d (8.65)	4S (0.27) 3d (9.51)	4S (0.35) 3d (9.99)

Figure Captions

Fig. 1. Chemical structures of cryptands L^1 and L^2 and their gas-phase optimised structures calculated using the B3LYP/6-311+G(d,p) approach. The hydrogen atoms are omitted for clarity (see Supplementary Information for positions). Only the labels of key atoms are shown on the chemical structures. Blue atoms represent nitrogen, while red atoms denote oxygen.

Fig. 2. Optimized geometry of $[Cu_2L^2]^{4+;}$ the hydrogen atoms are omitted and the carbons atoms around four-fold coordinated metal ions are in stick form for clarification.

Fig. 3**.** Dependence of cavity size (M…M distance) of dimetallic cryptates on the ionic radius of metal cation.

Fig. 4. Optimized geometry of $[Zn_2L^1CO_3]^{2+}$, $[Cu_2L^1CO_3]^{2+}$ and $[Ni_2L^2CO_3]^{2+}$ compounds. The hydrogen and carbons atoms around the coordination centre are in stick form for clarification.

Fig. 5 Correlation plot between experimental M…M distance and the results calculated in this work.

Fig. 6**.** Syn-anti μ-η_1, η_2 arrangement of methoxycarbonate arrangement within the host cavity of $[Cu_2L^1MeCO_3]^{3+}$.

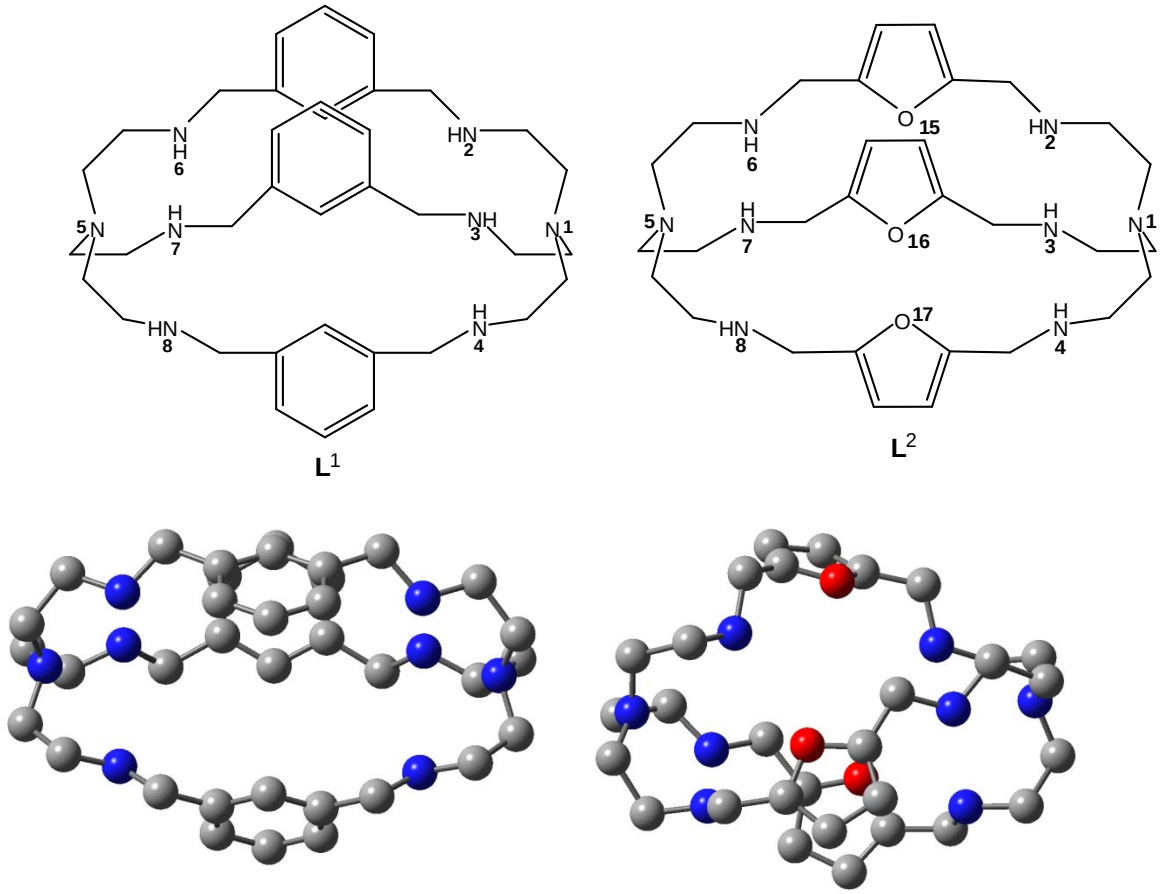

L^1 L^2

Fig. 1

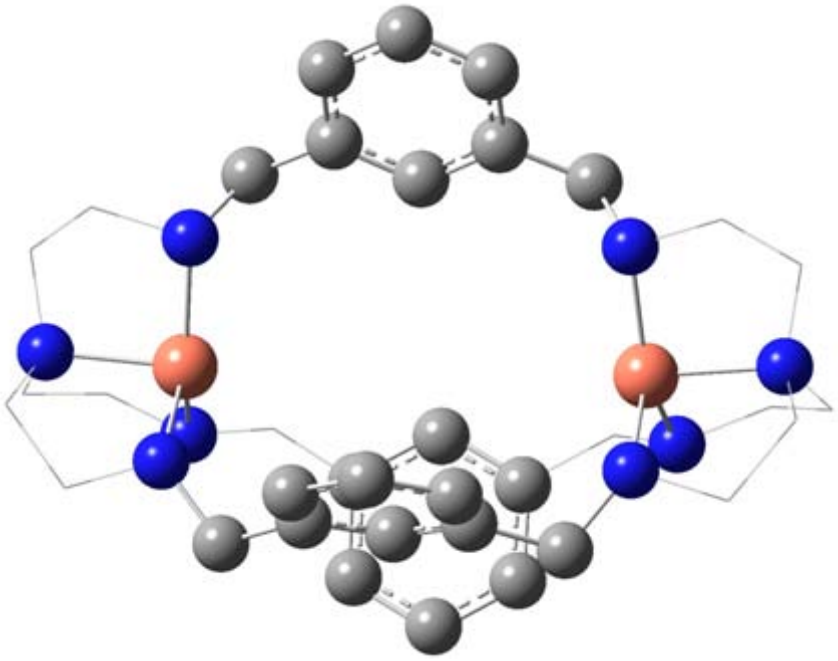

Fig. 2

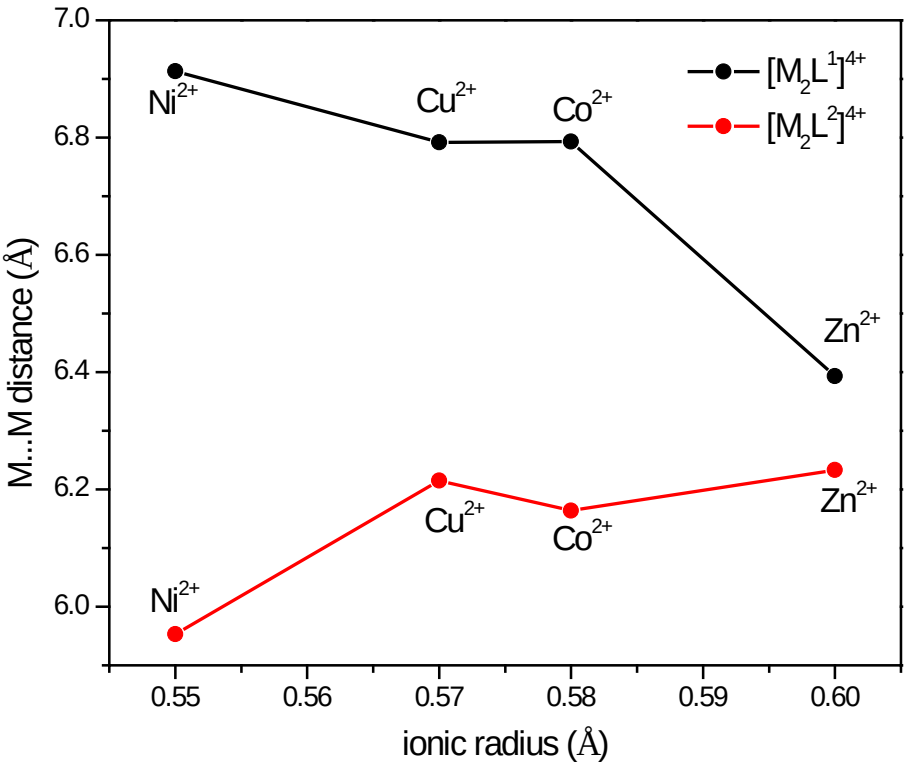
7.0
6.8
6.6
6.4
6.2
6.0
M...M distance (Å)
0.55
0.56
0.57
0.58
0.59
0.60
ionic radius (Å)
[M2L1]4+
[M2L2]4+
Ni2+
Cu2+
Co2+
Zn2+
Zn2+
Cu2+
Co2+
Ni2+

Fig. 3

$[Zn_2L^1CO_3]^{2+}$ $[Cu_2L^1CO_3]^{2+}$ $[Ni_2L^2CO_3]^{2+}$

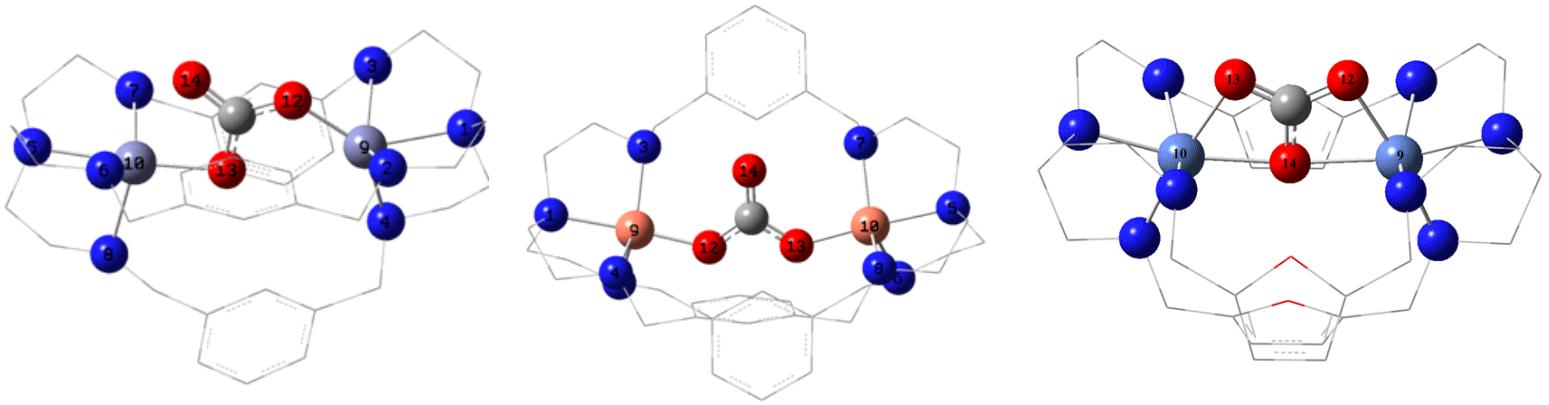

Fig. 4

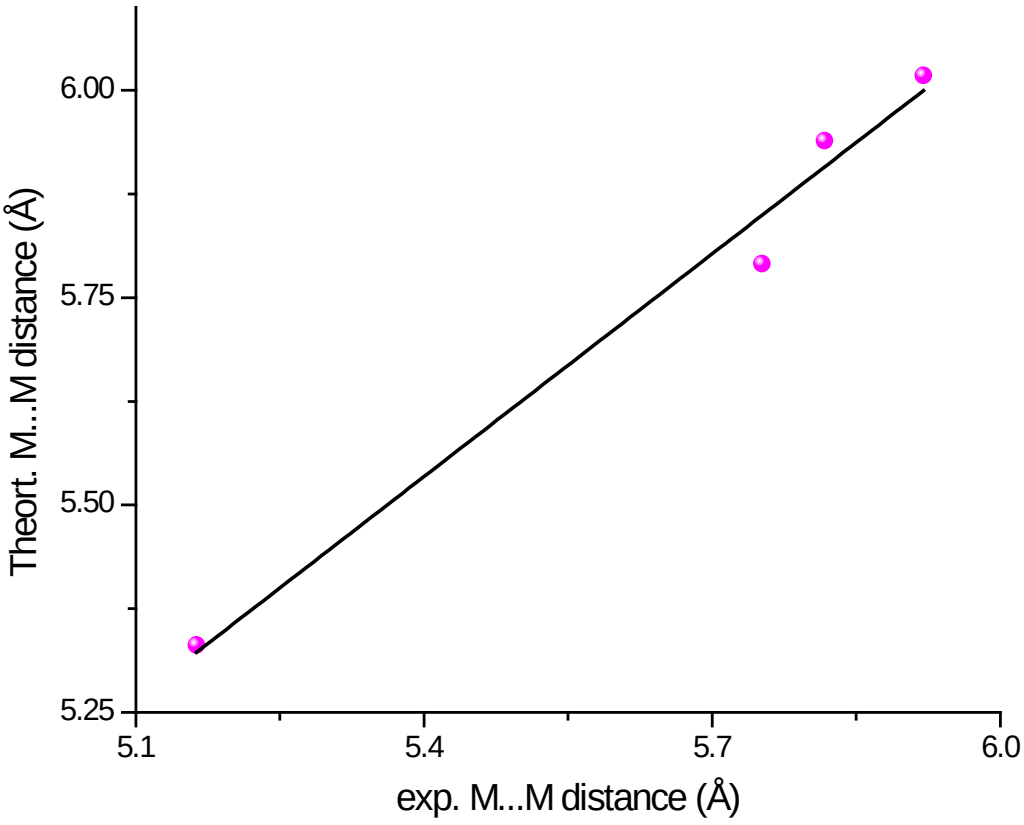
6.00
5.75
5.50
5.25
Theort. M...M distance (Å)
5.1
5.4
5.7
6.0
exp. M...M distance (Å)

Fig. 5

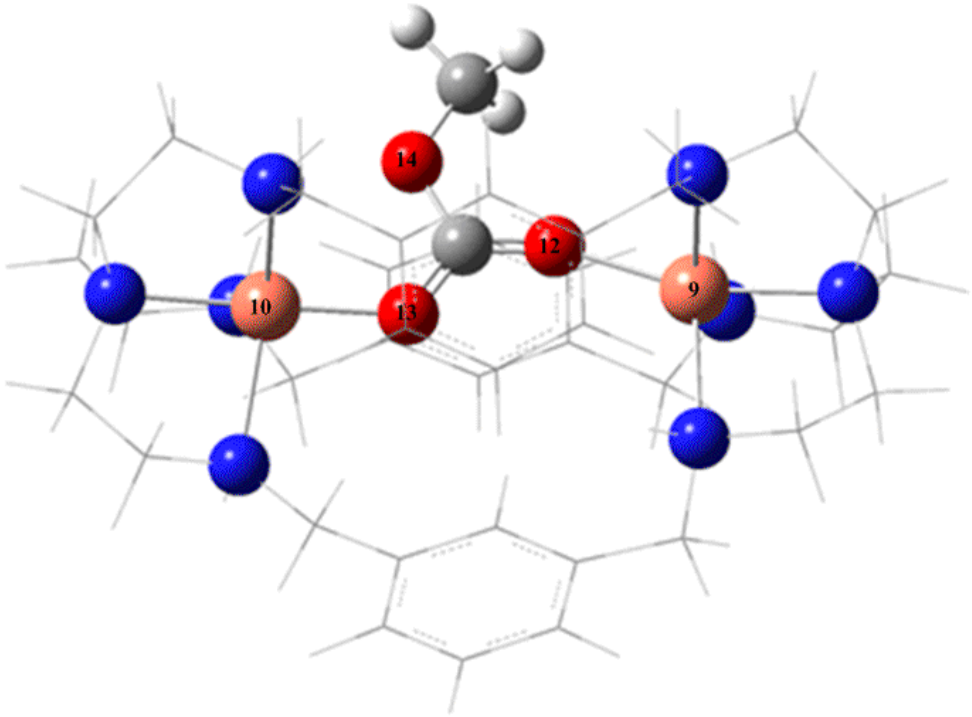

Fig. 6

Supplementary Information for

A Theoretical Thermodynamic Investigation of Cascade Reactions to Uptake Atmospheric Carbon Dioxide in Dinuclear Octa-azcryptates

Morad M. El-Hendawy, Niall J. English* and Damian A. Mooney

* Corresponding author: niall.english@ucd.ie

Table S1. The energies of dinuclear complexes at different spin states

$[M_2L]^{4+}$					
L1	Singlet	Triplet	Quintet	Septet	AF-singlet*
Co^{2+}	-4871.9357365	-4871.9544356	-4871.9629819	-4871.9741011	-4871.9743011
Ni^{2+}	-4858.1235187	-4858.1697459	-4858.2166841	---	-4858.2166893
Cu^{2+}	-5122.4691182	-5122.5232945	---	---	-5122.523296
L2					
Co^{2+}	-4600.3025729	-4600.3974605		-4600.4579712	-4600.4589712
Ni^{2+}	-4851.426834	-4851.479906	-4851.5286961	---	-4851.5286995
Cu^{2+}	-5115.7926132	-5115.8535429	---	---	-5115.8535517
$[M_2LCO_3]^{2+}$					
L1	Singlet	Triplet	Quintet	Septet	AF-singlet*
Co^{2+}	-4871.7938182	-4871.8893527	-4871.90986	-4871.9248429	-4871.9745542
Ni^{2+}	-5122.940036	-5122.9509821	-5122.9781888	---	-5122.9785698
Cu^{2+}	-5387.2660379	-5387.3130239	---	---	-5387.3670891
L2					
Co^{2+}	-4865.1667312	-4865.2526498	-4865.2688794	-4865.289254	-4865.3245084
Ni^{2+}	-5116.1942743	-5116.2849938	-5116.3624171	---	-5116.3639005
Cu^{2+}	-5380.6211838	-5380.6545882	---	---	-5380.6578638
$[M_2L^1MeCO_3]^{2+}$					
L1	Singlet	Triplet	Quintet	Septet	AF-singlet*
Co^{2+}	-4911.357907	-4911.4544356	-4911.4745366	-4911.4928595	-4911.4934002
Ni^{2+}	-5162.49588	-5162.5266524	-5162.5551128	---	-5162.5551389
Cu^{2+}	-5426.8018337	-5426.8680265	---	---	-5426.8679983

* AF-singlet=Antiferromagentic spin singlet state

Table S2. Optimized Cartesian coordinates (Å) for cryptands L^1 and L^2 at the B3LYP/6-311G+(d,p) Level

L^1

	x	y	z
N	-5.26676246	0.01408335	-0.02021091
N	-3.52272431	-0.23255873	2.45206767
N	-3.46522819	2.24050099	-1.03548766
N	-3.48084905	-1.99580193	-1.44067252
N	5.26368680	-0.01380273	0.02569365
N	3.46107989	-0.25186283	2.46190849
N	3.49490166	-2.01386873	-1.42479706
N	3.51182934	2.24464706	-0.99945925
C	-2.57162561	0.37540115	3.38268154
C	2.48865068	0.38623354	3.34869257
C	-0.04127486	0.29646136	3.33511137
C	-1.26009553	-0.38134504	3.43107139
C	1.18138252	-0.37775231	3.41026971
C	-1.24556058	-1.77038149	3.59088353
C	1.17369539	-1.76657395	3.56954822
C	-4.82048008	0.43384516	2.41272352
C	-0.03436044	-2.45532216	3.65817409
C	4.76643350	0.40108280	2.44870610
C	5.68560890	-0.25118264	1.41796218
C	-5.72545880	-0.20758375	1.36290951
C	0.00797517	4.40570557	0.28883877
C	-1.19315639	3.97302352	-0.26963703
C	1.22580460	4.01037768	-0.25977408
C	4.79475062	-2.32311030	-0.83729116
C	-5.69111742	1.33098445	-0.52782929
C	5.70711181	-1.09871768	-0.86777626
C	5.71638400	1.30262210	-0.45843934
C	-4.78610084	-2.29947667	-0.86195328
C	-5.69740712	-1.07502943	-0.91495688
C	2.53660920	-3.11712095	-1.35691525
C	-2.52382198	-3.09893220	-1.35747241
C	0.00666785	-3.03890404	-1.41516627
C	-1.18718472	3.13399310	-1.38759200
C	1.25431243	3.17140943	-1.37799239
C	-4.76400287	1.89230897	-1.60369589
C	4.81881386	1.89127456	-1.54466849
C	1.22859696	-2.77912494	-2.04282013
C	-1.21314777	-2.76985028	-2.04312728
C	-2.48700601	2.68866217	-2.02645959
C	0.04236080	2.73605873	-1.92191192
C	2.57377262	2.75959082	-1.99743512
C	1.21979597	-2.22014733	-3.32418856
C	-1.19966644	-2.21100476	-3.32447627
C	0.01123515	-1.93816107	-3.95745132
H	0.01296518	-1.50633059	-4.95290365
H	-3.03427884	0.35997980	4.37810243

H	2.93392284	0.41807050	4.35170343
H	-5.29524754	0.31766288	3.39410360
H	5.21996936	0.28187502	3.43971818
H	-0.04413403	1.37348895	3.19158403
H	-2.18627332	-2.30525990	3.65137648
H	-2.37042366	1.43524427	3.15282161
H	2.11711590	-2.29803095	3.61392233
H	-0.03149587	-3.53311903	3.78378107
H	2.28301477	1.43348893	3.07061387
H	-4.73446468	1.51939257	2.23163763
H	4.69500354	1.48686127	2.26345939
H	5.67608196	-1.32699259	1.60371145
H	-5.73847381	-1.28237700	1.55414808
H	6.72181230	0.09498185	1.57466974
H	-6.75915465	0.15669721	1.49315301
H	-0.00568314	5.05830957	1.15563498
H	3.09615838	-0.27345110	1.51400649
H	-3.12793061	-0.24059839	1.51611423
H	4.71305732	-2.71401426	0.19177662
H	-2.14162644	4.27361061	0.16001453
H	-4.71391008	-2.67754401	0.17255392
H	2.16095738	4.33935971	0.17860576
H	-5.69396281	2.03707795	0.30508782
H	5.71368810	1.99882804	0.38256666
H	6.74184145	-1.40117868	-0.63056712
H	2.33069188	-3.43915731	-0.32231489
H	-2.32125823	-3.40987935	-0.31884789
H	-6.73604241	-1.37493998	-0.69260589
H	-3.10039708	1.43602339	-0.53373277
H	0.00498948	-3.45500003	-0.41142049
H	3.11350413	1.42914120	-0.54307464
H	5.26177108	-3.11461071	-1.43507746
H	-6.72329284	1.28470727	-0.91603592
H	6.75507760	1.24532048	-0.82735579
H	3.11018279	-1.19693513	-0.95952936
H	-5.24718033	-3.09805165	-1.45489043
H	-3.09917132	-1.17629052	-0.97736345
H	2.99562601	-3.97784702	-1.86051274
H	-2.98199977	-3.96480714	-1.85293830
H	5.71158621	-0.71983914	-1.89169449
H	-5.68498675	-0.70242198	-1.94109163
H	-5.21782198	2.80474418	-2.00801993
H	5.29094781	2.80576172	-1.92249583
H	-4.68180301	1.18265240	-2.44521915
H	4.74815811	1.19775235	-2.40067825
H	-2.27228168	1.92163749	-2.78930203
H	3.04306594	3.63667565	-2.46160781
H	-2.93272203	3.53686437	-2.56229731
H	2.38437424	2.04243518	-2.81368148
H	0.05601404	2.07010956	-2.78040702
H	2.16266654	-2.00069313	-3.81161087
H	-2.14073054	-1.98462447	-3.81214134

N	-4.72548000	0.03669700	-0.41826600
N	-2.68819500	2.24728700	0.50961400
N	-2.63706500	-1.17627500	-2.07785300
N	-3.08913400	-2.01801300	1.05865800
N	4.73489900	0.21902900	-0.06068300
N	2.31577600	1.67087400	-1.37162800
N	2.74572300	0.19296000	2.07791700
N	3.18066200	-2.36877600	-0.01774700
O	-0.22774200	3.23773400	-0.99578900
O	-0.78583900	-0.44169100	2.43991100
O	0.88660500	-1.93526400	-1.98883700
C	-4.97688800	1.43922000	-0.10986500
C	-4.04968400	2.00616700	0.97638900
C	-4.90628800	-0.31982500	-1.82602700
C	-2.45827500	3.59140400	-0.02367900
C	-3.59432300	-0.20987600	-2.60517200
C	-5.28068000	-0.90106000	0.54627600
C	-1.01242700	3.93447400	-0.11339300
C	-0.24979400	4.85148900	0.54307800
C	1.08638900	4.71086200	0.04397100
C	1.05063500	3.71677900	-0.88367400
C	-4.48630300	-2.21310100	0.67634600
C	-1.29758200	-1.05098100	-2.63811000
C	2.09172900	3.07347500	-1.73203800
C	-2.86093800	-1.74576700	2.48170500
C	-0.43764200	-2.19973900	-2.21328700
C	-1.41245300	-1.60802900	2.80063300
C	-0.68175400	-3.52194600	-2.00238900
C	1.41376500	0.62433000	2.49283000
C	3.68885100	1.29698300	1.91232000
C	0.53593700	-0.55328300	2.78103100
C	3.46769500	1.06502000	-2.04132400
C	-0.50418800	-2.44896200	3.36767300
C	0.56994400	-4.11168900	-1.62471300
C	1.49334500	-3.11183200	-1.62721300
C	4.74084000	1.15003800	-1.18152400
C	0.75795100	-1.76865000	3.35305300
C	4.97738700	0.78247000	1.26320900
C	2.94173500	-3.06387900	-1.28511900
C	5.30887900	-1.08864100	-0.33022400
C	4.58288400	-2.24901600	0.37358000
H	5.15781300	-3.17327200	0.18006500
H	-6.02752200	1.60435900	0.19841500
H	-4.83160000	2.02229900	-1.02276900
H	-5.67755600	0.30534100	-2.30366300
H	-4.51022100	2.92935800	1.37307000
H	-2.92858700	4.37285600	0.59893300
H	-2.91904900	3.66563900	-1.01688700
H	-3.22291400	0.82842200	-2.54648800
H	-3.78069800	-0.42860400	-3.66434600
H	-6.33062600	-1.16634600	0.31504300
H	-4.00395100	1.30255000	1.81092100
H	-5.25580000	-1.35369200	-1.89350700
H	-0.60003500	5.54351700	1.29315700
H	-5.30917600	-0.40745000	1.52114700
H	-2.01101400	2.02935400	1.22962500

H	-2.59363000	-1.06241300	-1.06385300
H	-1.38275300	-1.04109700	-3.73309200
H	1.95982900	5.26900500	0.34273200
H	-4.48643400	-2.72868000	-0.28696000
H	-0.79097800	-0.11123400	-2.35942000
H	-5.03340900	-2.86118600	1.38584500
H	1.83246000	3.19500500	-2.79966800
H	-3.37653200	-0.81691700	2.74439600
H	3.02152000	3.62683000	-1.57338800
H	2.67553300	-0.29038600	1.18169600
H	-3.27735000	-2.53367100	3.13323400
H	-2.53189400	-2.81647400	0.77559400
H	0.91078100	1.26123600	1.74720400
H	-1.63820400	-4.00650100	-2.11150300
H	1.47606400	1.12845200	-1.53346400
H	3.27131400	2.10679200	1.29190400
H	3.92561800	1.72014200	2.89701000
H	3.66262100	1.53492100	-3.02131600
H	4.83290200	2.16948000	-0.79389300
H	1.51955800	1.23414700	3.40011300
H	3.24152900	0.01404800	-2.23200200
H	-0.71050000	-3.43792300	3.74801100
H	2.63770900	-2.80546600	0.71836900
H	0.75917400	-5.14547900	-1.37864500
H	5.71866400	1.59810800	1.22692800
H	5.62091700	0.98713400	-1.82715100
H	5.39848100	0.00346600	1.90488700
H	1.70661400	-2.12186400	3.72325400
H	3.48429000	-2.53570600	-2.07628000
H	4.60651000	-2.08212200	1.45300100
H	3.32199400	-4.10000700	-1.28236200
H	5.27256400	-1.25482300	-1.41046800
H	6.37899400	-1.14246600	-0.05186700

Table S3. Lengths (Å) of newly formed bonds due to the encapsulation of two metal cations in the host cavity of the respective cryptands.

	$[M_2L^1]^{4+}$				$[M_2L^2]^{4+}$			
	Co^{2+}	Ni^{2+}	Cu^{2+}	Zn^{2+}	Co^{2+}	Ni^{2+}	Cu^{2+}	Zn^{2+}
M9-N1	2.091	2.030	2.020	2.083	2.090	2.025	2.048	2.085
M9-N2	2.047	2.039	2.023	2.054	2.094	2.116	2.000	2.086
M9-N3	2.062	2.046	2.028	2.070	2.056	2.027	1.993	2.045
M9-N4	2.074	2.038	2.174	2.042	2.078	2.077	2.280	2.078
M10-N5	1.959	2.039	2.020	2.087	2.090	2.025	2.069	2.085
M10-N6	2.146	2.062	2.023	2.061	2.094	2.116	2.344	2.086
M10-N7	2.000	2.067	2.028	2.068	2.056	2.027	2.035	2.045
M10-N8	2.000	2.071	2.028	2.049	2.078	2.077	2.039	2.045
M9-M10	6.793	6.913	6.792	6.393	6.164	5.953	6.215	6.233

Table S4. Binding Gibbs free energies of the three approaches listed below at 298.15 K for (i) $[M_2L^1]^{4+}$ and (ii) $[M_2L^2]^{4+}$ complexes

(i)	ΔG_{app1}	ΔG_{app2} [a]	ΔG_{desolv}	ΔG_{app3}	**Overall stability constant**
Co^{2+}	-467	287970	278	-189	13.56[a]
Ni^{2+}	-513	287892	288	-225	---
Cu^{2+}	-567	287882	296	-271	26.20[a]
Zn^{2+}	-517	287685	173	-344	---
(ii)	ΔG_1	ΔG_1	ΔG_{desolv}	ΔG_{app3}	---
Co^{2+}	-458	287955	278	-180	9.75 ± 0.06[b]
Ni^{2+}	-496	287936	288	-208	---
Cu^{2+}	-564	287936	296	-268	25.38 ± 0.08[b]
Zn^{2+}	-514	287885	173	-341	16.10 ± 0.01[b]

[a] The value of ΔG_{app2} are large and positive, and therefore unacceptable.
[a] and [b] refer to data taken from refs. [21] and [33], respectively.

First approach (ΔG_{app1}): $2M^{2+} + L \xrightarrow{\Delta G_1} [M_2L]^{4+}$

Second approach (ΔG_{app2}): $2[M(H_2O)_6]^{2+} + L \xrightarrow{\Delta G_1} [M_2L]^{4+} + 6H_2O$

Third approach ($\Delta G_{app3} = \Delta G_1 + \Delta G_{desolv}$):

$[M(H_2O)_6]^{2+} \xrightarrow{\Delta G_{desolv}} 2M^{2+} + 6H_2O$ Then $2M^{2+} + L \xrightarrow{\Delta G_1} [M_2L]^{4+}$

Tables S5, S6 and S7 show selected bond lengths and bond angles of the optimized structures of the complexes together with available experimental X-ray data, where available.

Table S5. Selected bond distances (Å) and angles (º) of $[M_2L^1CO_3]^{2+}$, together with the corresponding experimental data in brackets (taken from ref [9])

	Co^{2+}	Ni^{2+}	Cu^{2+}	Zn^{2+}
M9-N1	2.267 (2.191)	2.099 (2.081)	2.067 (2.032)	2.231 (2.232)
M9-N2	2.167 (2.161)	2.195 (2.151)	2.299 (2.232)	2.219 (2.188)
M9-N3	2.170 (2.127)	2.203 (2.126)	2.093 (2.074)	2.346 (2.178)
M9-N4	2.174 (2.110)	2.088 (2.126)	2.156 (2.061)	2.118 (2.095)
M10-N5	2.240 (2.193)	2.092 (2.106)	2.067 (2.048)	2.264 (2.268)
M10-N6	2.175 (2.158)	2.109 (2.136)	2.299 (2.227)	2.204 (2.159)
M10-N7	2.197 (2.148)	2.248 (2.243)	2.093 (2.120)	2.246 (2.137)
M10-N8	2.200 (2.123)	2.128 (2.124)	2.156 (2.090)	2.184 (2.100)
M9...M10	5.855 (5.939)	5.920 (6.018)	5.762 (5.791)	5.163 (5.331)
M9-O12	1.870 (1.904)	1.877 (1.946)	1.863 (1.872)	1.936 (1.979)
M10-O13	1.890 (1.920)	1.892 (1.969)	1.863 (1.875)	2.002 (1.989)
M9-O12-C11	125.3 (139.6)	135.5 (140.3)	131.4 (135.3)	124.8 (133.6)
M10-O13-C11	142.4 (137.7)	128.2 (137.7)	131.4 (131.5)	111.89 (120.2)

Table S6. Selected bond distances (Å) and angles (º) of $[M_2L^2CO_3]^{2+}$, together with the corresponding experimental data in brackets (taken from ref [9])

	Co^{2+}	Ni^{2+}	Cu^{2+}	Zn^{2+}
M9-N1	2.222 (2.157)	2.125	2.123	2.198
M9-N2	2.176 (2.165)	2.221	2.422	2.267
M9-N3	2.262 (2.236)	2.124	2.029	2.145
M9-N4	2.312 (2.261)	2.269	2.381	2.368
M10-N5	2.222 (2.177)	2.077	2.123	2.198
M10-N6	2.176 (2.154)	2.077	2.422	2.268
M10-N7	2.262 (2.205)	2.218	2.029	2.143
M10-N8	2.312 (2.247)	2.218	2.381	2.370
M9...M10	4.406 (4.292)	4.427	4.336	4.429
M9-O12	2.110 (2.145)	2.077	2.004	2.104

M10-O13	2.110 (2.145)	2.077	2.004	2.039
M9-O14	2.206 (2.151)	2.218	2.177	2.210
M10-O14	2.205(2.157)	2.218	2.177	2.226
M9-O12-C11	93.5 (93.3)	94.1	94.0	93.5
M10-O13-C11	93.5 (92.4)	94.1	94.0	94.2
M9-O14-C11	88.0 (90.7)	86.9	85.5	87.6
M10-O14-C11	88.0 (90.0)	86.9	85.5	87.1

Table S7. Selected bond distances (Å) and angles (º) of $[M_2L^1MeCO_3]^{3+}$, together with the corresponding experimental data in brackets (taken from ref [9])

	Co^{2+}	**Ni^{2+}**	**Cu^{2+}**	**Zn^{2+}**
M9-N1	2.228	2.104 (2.084)	2.086 (2.034)	2.247 (2.279)
M9-N2	2.142	2.099 (2.085)	2.091 (2.040)	2.122 (2.291)
M9-N3	2.166	2.144 (2.139)	2.301 (2.232)	2.155 (2.138)
M9-N4	2.177	2.166 (2.081)	2.124 (2.074)	2.160 (2.152)
M10-N5	2.230	2.111 (2.032)	2.073 (2.061)	2.228 (2.192)
M10-N6	2.144	2.089 (2.121)	2.245 (2.158)	2.140 (2.117)
M10-N7	2.165	2.130 (2.102)	2.161 (2.086)	2.189 (2.155)
M10-N8	2.183	2.197 (2.088)	2.133 (2.034)	2.197 (2.168)
M9-O12	2.025	2.039 (2.011)	1.978 (1.941)	2.051 (2.099)
M10-O13	2.004	2.014 (2.050)	2.014 (1.963)	2.039 (2.062)
M9-O12-C11	123.9	121.0 (121.1)	123.1 (120.3)	127.7 (125.5)
M10-O13-C11	141.2	142.4 (141.9)	146.1 (151.9)	153.0 (154.5)
M9...M10	5.591	5.648 (5.629)	5.667 (5.655)	5.888 (5.982)